J Therm Anal Calorim (2011) 103:479–484
DOI 10.1007/s10973-010-1016-1

The effect of ball-milling on the thermal behavior of anatase-doped hematite ceramic system

Monica Sorescu · Tianhong Xu

Received: 12 April 2010 / Accepted: 18 August 2010 / Published online: 29 August 2010

Abstract High energy ball-milling methods were employed in the synthesis of anatase-doped hematite $x\text{TiO}_2(\text{a}) \cdot (1-x)\alpha\text{-Fe}_2\text{O}_3$ ($x = 0.1$, 0.5, and 0.9) ceramic system. The thermal behavior of as obtained ceramic system was characterized by simultaneous DSC–TG. The pure anatase phase was found to be stable below 800 °C, but there is a 10.36% mass loss due to the water content. Two exothermic peaks on DSC curves of pure anatase indicate the different crystallization rates. The pure hematite partially decomposed upon heating under argon atmosphere. Ball-milling has a strong effect on the thermal behaviors of both anatase and hematite phases. For $x = 0.1$ and 0.5, there is gradual Ti substitution of Fe in hematite lattice, and the decomposition of hematite is enhanced due to the smaller particle size after ball-milling. The crystallization of hematite was suppressed as the enthalpy values decreased due to the anatase-hematite solid–solid interaction. For $x = 0.9$, most of the anatase phase converted to rutile phase after long milling time. The thermal behavior of $x\text{TiO}_2(\text{a}) \cdot (1-x)\alpha\text{-Fe}_2\text{O}_3$ showed smaller enthalpy value of the hematite transformation to magnetite and anatase crystallization due to the small fraction of hematite phase in the system and hematite–anatase interaction, while the mass loss upon heating increased as a function of milling time due to more water content absorbed by the smaller particle size.

M. Sorescu (✉) · T. Xu
Department of Physics, Duquesne University,
Bayer Center, Pittsburgh, PA 15282-0321, USA
e-mail: sorescu@duq.edu

Keywords Anatase-doped hematite · Ball-milling · Simultaneous DSC–TG · Crystallization · Enthalpy

Introduction

TiO_2 and Fe_2O_3 can be found in wide applications, such as catalysts [1] and gas sensors [2, 3]. Recently, binary mixed oxides were reported to be good catalysts with improved photocatalytic properties and enhancement of visible light response. Studies with a novel TiO_2–Fe_2O_3 mixed oxide catalyst have shown an increased photocatalytic activity for dichloroacetic acid destruction at 450 nm [4]. The photocatalytic activity of TiO_2–Fe_2O_3 mixed oxide with different proportions of Fe_2O_3 and TiO_2, prepared by impregnation and co-precipitation methods, has been shown to be active in the visible light for the photoreduction of N_2 [5], degradation of oligocarboxylic acid [6], photodegradation of 4-nitrophenol [7], and $CHCl_3$ oxidation [8]. The catalytic activities of TiO_2–Fe_2O_3 largely depend on preparation methods, iron content, calcination temperature, and phase composition. Therefore, the thermal behaviors of TiO_2 and Fe_2O_3 are widely studied [9–11].

High energy ball-milling is a low cost, simple operation method for preparing extended solid solutions and nanoparticle systems. To the best of our knowledge, there is no literature available on the ball-milling effect on thermal behavior of mixed oxide nanoparticles.

In this work, $x\text{TiO}_2(\text{a}) \cdot (1-x)\alpha\text{-Fe}_2\text{O}_3$ (with molar concentration $x = 0.1$, 0.5, and 0.9) ceramic system was synthesized through high energy ball-milling. The thermal behaviors of these as-obtained samples were studied by simultaneous DSC–TG. The difference in thermal behavior between ball-milled nanoparticles, original hematite, and anatase was presented. The thermal behaviors of the

ceramic system in connection with anatase concentration after ball-milling were discussed.

Experimental

The details of the preparation of $x\mathrm{TiO_2(a)} \cdot (1-x)\alpha\text{-}\mathrm{Fe_2O_3}$ ceramic system, along with the X-ray and Mössbauer spectroscopy results have been described in [12]. Powders of hematite and anatase were milled at different molar concentrations ($x = 0.1$, 0.5, and 0.9) in a hardened steel vial with 12 stainless-steel balls (type 440; eight of 0.25 in diameter and four of 0.5 in diameter) in the SPEX 8000 mixer mill for time periods ranging from 2 to 12 h. The ball/powder mass ratio was 5:1 and all ball-milling experiments were performed in a glove box under protective argon atmosphere. The average particle sizes of starting hematite and anatase are $\sim$60 and $\sim$10 nm, respectively. After ball milled for 12 h, the average particle size of hematite and anatase decreased to $\sim$15 and $\sim$8 nm, as estimated from XRD patterns using Scherrer equation. The milling product for $x = 0.1$ is $\mathrm{TiO_2(a)}$-doped hematite phase after 2 h ball-milling, while for $x = 0.5$ and 0.9, the milling products are mixtures of $\mathrm{TiO_2(a)}$-doped hematite phase and hematite-doped anatase phase, as identified from XRD and Mössbauer measurements.

Simultaneous DSC–TG experiments were performed using a Netzsch Model STA 449F3 Jupiter instrument with a Silicon Carbide (SiC) furnace. Samples were contained in a manufacturer's alumina crucible with an alumina lid. Experiments were performed using 12 ± 1 mg sample size. The atmosphere was flowing protective argon gas at a rate of 50 ml $\mathrm{min^{-1}}$. DSC and TG curves were obtained by heating samples from room temperature to 800 °C with a rate of 10 °C $\mathrm{min^{-1}}$. Both DSC and TG curves were corrected by subtraction of baselines which was run under identical conditions as DSC–TG measurement, with residue of samples in the crucible. The Netzsch Proteus Thermal Analysis software was used for DSC–TG data analysis.

Results and discussion

The DSC curve of original hematite sample (Fig. 1a) showed an exothermic peak at 358 °C. There is another exothermic peak which starts at 600 °C and is not completed over the considered temperature range. The existence of double peaks in the DSC curve indicates that hematite is not stable and undergoes a two-step phase transformation mechanism under high temperature and argon atmosphere. The first phase change completes below 600 °C, while the second phase change starts at 600 °C.

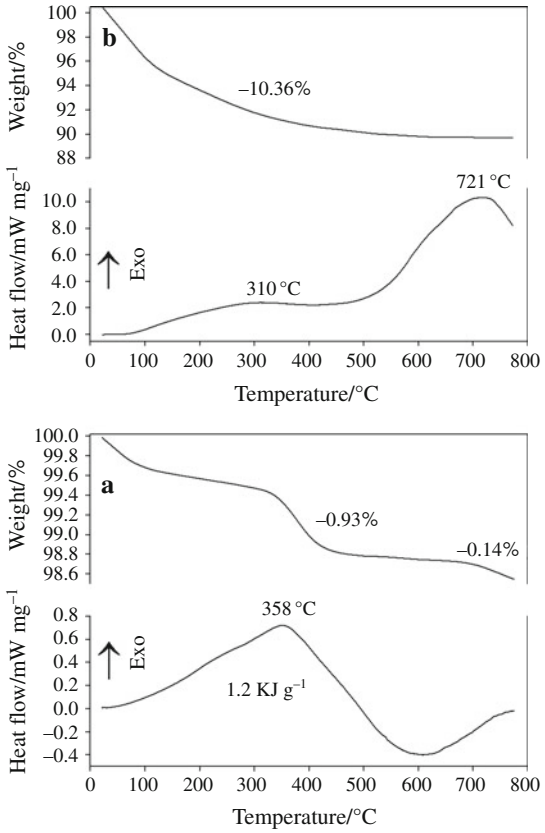

Fig. 1 TG–DSC curves of original **a** hematite; **b** anatase

These two phase transformations are completely separated, indicating that the second phase transformation occurs after the completion of the first phase transformation. Integration of the first peak gives an enthalpy value of 1.2 kJ $\mathrm{g^{-1}}$. No exact enthalpy value can be extracted for the second phase transformation.

The thermal behavior of the original hematite sample was also investigated using TG analysis. As can be seen in Fig. 1a, the thermogravimetry of hematite reveals two major mass losses: one is in a relatively low temperature range from 300 to 450 °C, and the other starts above 650 °C. These two mass losses are probably due to the thermal decomposition of hematite. The first mass loss is possibly related to the decomposition of hematite to magnetite. The second mass loss is mainly caused by the further decomposition of magnetite to wüstite.

These two mass losses are in good agreement with the DSC curve of the original hematite, which shows one exothermic peak and with a sign of a second peak being under development above 600 °C. The first phase transformation in the DSC curve with a broad peak below 600 °C corresponds to the first mass loss, and the peak temperature of DSC curve at 358 °C is exactly the same as that of TG curve where the first mass loss occurs. It has been reported that hematite completely decomposed to

magnetite in the presence of high boiling point solvent 1-octadecence under N_2 atmosphere at 320 °C for 28 h refluxing [13]; this temperature is in the temperature range of our DSC exothermic peak. Comparing with the broad temperature range of DSC curve, the mass loss occurs in a relatively small temperature range, indicating that the mass loss occurs simultaneously with the crystallization of hematite fine particles. The second mass loss starts around 650 °C, and the DSC curve shows a rising value of heat flow.

The first mass loss determined from the TG curve of the original hematite is 0.93%, which is much less than the theoretical mass loss value of 3.44% as calculated from equation $3Fe_2O_3 \rightarrow 2Fe_3O_4 + 1/2O_2$, indicating that only a part of hematite decomposes to magnetite. The partial decomposition of hematite is probably due to Ar impurifications. Moreover, the possible existence of oxygen partial pressure may affect the equilibrium of hematite thermal decomposition reaction. It was also reported that hematite partially decomposes with release of gaseous oxygen under helium atmosphere with a pressure of 250–700 Pa [14]. All these point to the relative stability and difficulty of decomposition of hematite in the presence of argon. The small mass losses up to temperatures of ~100 °C for all the studied samples can be attributed to the surface physically adsorbed water.

The DSC–TG curve of original anatase sample is shown in Fig. 1b, in which two exothermic peaks can be seen. The first broad exothermic peak is at ~310 °C, while the other is at 721 °C. TG curve of anatase shows that there is a gradual mass loss up to 500 °C. The original anatase and anatase sample annealed at 800 °C for 1 h under Ar atmosphere were confirmed to be 100% pure anatase by XRD measurements. The mass loss is assigned to the water content in the original anatase sample, and these two exothermic peaks are not related to the phase transformation between anatase and rutile. By analyzing the particle size as a function of annealing temperature obtained from XRD patterns using Scherrer equation, it was found that the average particle size of anatase increased slowly below 550 °C, with values of ~10 nm at room temperature and ~12 nm at 550 °C. However, it increased sharply when anatase was annealed at 650 and 750 °C, with values of ~18 and 27 nm, respectively. The possible explanation of these two exothermic peaks is that they are due to the crystallization of amorphous anatase at different rates. The XRD patterns of anatase annealed at 650 and 750 °C also confirmed a steep enhancement in crystallinity with obvious separation of two additional peaks at 2θ of 36.88° and 38.50°. Due to the simultaneous processes of water loss and crystallization under heating, no endothermic peak associating with water loss was observed.

Figure 2a–e shows the DSC curves of $x\text{TiO}_2(a) \cdot (1-x)\alpha\text{-Fe}_2\text{O}_3$ samples ($x = 0.1$) after ball-milling for 0, 2, 4, 8, and 12 h, respectively. At 0 h milling, the DSC curve showed one broad peak (Fig. 2a) with the peak temperature at 509 °C. The characteristic of this peak differs from DSC curves of original hematite and anatase samples. The integration of this peak gives an enthalpy value of 2.29 kJ g^{-1}, which is much higher than that of the original hematite. This means that the manually ground mixture of $x\text{TiO}_2(a) \cdot (1-x)\alpha\text{-Fe}_2\text{O}_3$ ($x = 0.1$) shows different thermal behavior from hematite or anatase alone. This may characterize solid–solid interaction between hematite and anatase and/or the phase transformation process of hematite decomposition.

Figure 3a shows the TG curve of $x\text{TiO}_2(a) \cdot (1-x)\alpha\text{-Fe}_2\text{O}_3$ ($x = 0.1$) for 0 h ball-milling. 0.93% mass loss can be observed with temperature up to 600 °C, which is similar to that of the original hematite (0.93%). This means the manually grounding processes does not change the phase transformation of hematite decomposition. Comparing with pure hematite sample, the increase in the enthalpy for this

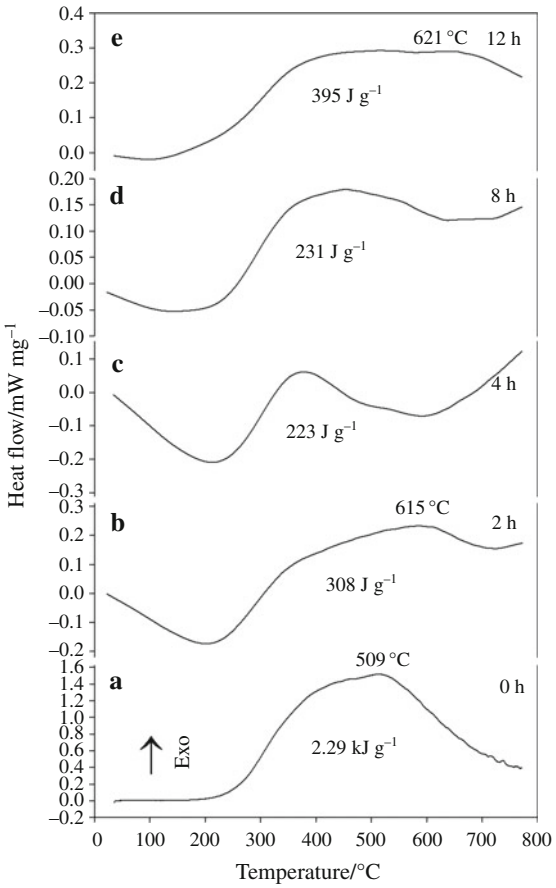

Fig. 2 DSC curves of $x\text{TiO}_2(a) \cdot (1-x)\alpha\text{-Fe}_2\text{O}_3$ ceramic system at $x = 0.1$ and ball-milling time of **a** 0 h; **b** 2 h; **c** 4 h; **d** 8 h; **e** 12 h

manually ground sample must be due to the addition of anatase.

After ball-milling for 2, 4, 8, and 12 h (Fig. 2b–e), the DSC curves of $x\mathrm{TiO_2(a)} \cdot (1-x)\alpha\text{-}\mathrm{Fe_2O_3}$ samples ($x = 0.1$) change dramatically compared to the 0 h milling sample, indicating the strong effect of ball-milling on the thermal behavior of $x\mathrm{TiO_2(a)} \cdot (1-x)\alpha\text{-}\mathrm{Fe_2O_3}$ system. The DSC curves are more likely flat and with much smaller enthalpy values, as indicated on the graphs. From the TG curves of $x\mathrm{TiO_2(a)} \cdot (1-x)\alpha\text{-}\mathrm{Fe_2O_3}$ samples ($x = 0.1$) after different ball-milling times (Fig. 3b–e), it was found there is slightly higher mass loss for each sample than that of 0 h milling sample, indicating hematite is less stable after ball-milling. Comparing with the manually ground sample, XRD results showed that the average particle sizes are smaller after milling, which decreased the stability of hematite upon heating under argon atmosphere. Mössbauer results [12] showed there are different types of magnetic species due to the gradual dissolution of anatase into hematite, and the thermal behavior of these hematite species is different from that of original hematite. The dramatic decrease in the enthalpy value is possibly due to Ti substitution of Fe in hematite lattice after milling, which suppresses the crystallization of hematite and anatase fine particles. The overall trend of decrease in enthalpy value as a function of milling time also confirmed that the increase of Ti substitution for Fe in hematite increases the $\mathrm{Fe_2O_3}$–$\mathrm{TiO_2}$ solid–solid interaction, which in turn suppresses the crystallization of fine particles.

Figure 4 shows peak temperature extracted from the DSC curves of $x\mathrm{TiO_2(a)} \cdot (1-x)\alpha\text{-}\mathrm{Fe_2O_3}$ samples ($x = 0.5$) after milling for 0, 2, 4, 8, and 12 h of milling time, respectively. At 0 h milling time, the DSC curve showed one broad peak with the peak temperature at 523 °C. The integration of this peak gives an enthalpy value of 1.79 kJ g^{-1}, which is much higher than that of the original hematite. This means that the manually ground mixture of anatase and hematite shows different thermal behaviors from samples with only hematite or anatase phase. Figure 5 shows mass loss extracted from the TG curve of $x\mathrm{TiO_2(a)} \cdot (1-x)\alpha\text{-}\mathrm{Fe_2O_3}$ sample ($x = 0.5$) after milling for 0, 2, 4, 8, and 12 h, respectively. A 0.81% mass loss can be observed with temperature up to 600 °C for 0 h milling sample, which is similar to that of the original hematite (0.93%). However, this also indicates that more hematite will decompose upon heating under argon atmosphere by considering the molar concentration $x = 0.5$. The increase in the enthalpy for this sample must be due to the addition of anatase.

After ball-milling for 2, 4, 8, and 12 h, the DSC curves of $x\mathrm{TiO_2(a)} \cdot (1-x)\alpha\text{-}\mathrm{Fe_2O_3}$ samples ($x = 0.5$) change dramatically, the peak temperature shifted to higher values (Fig. 4), indicating the strong effect of ball-milling on the thermal behavior. Comparing to 0 h milling sample, the DSC curves are more likely flat and with much smaller enthalpy, with values of 60 and 226 J g^{-1} after 2 and 12 h milling time, respectively. From the mass loss of $x\mathrm{TiO_2(a)} \cdot (1-x)\alpha\text{-}\mathrm{Fe_2O_3}$ samples ($x = 0.5$) after different milling times (Fig. 5), it was found that the mass loss for

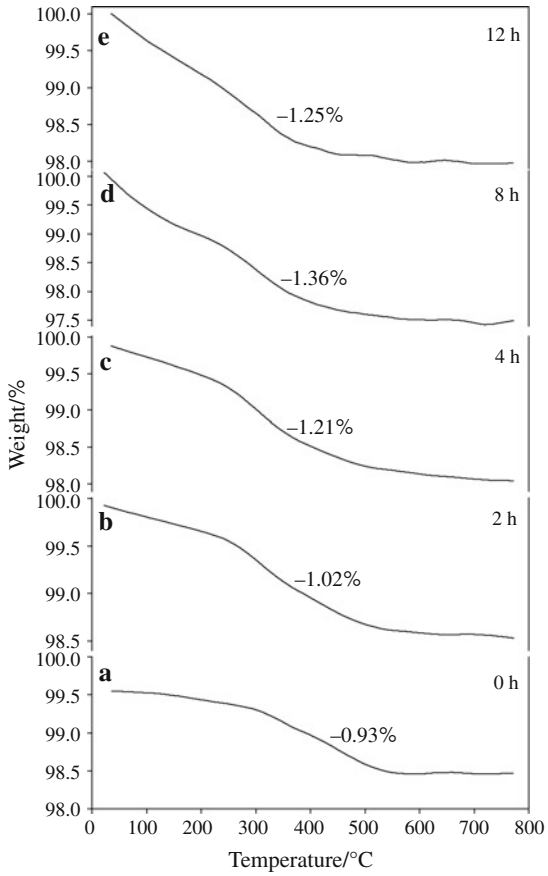

Fig. 3 TG curves of $x\mathrm{TiO_2(a)} \cdot (1-x)\alpha\text{-}\mathrm{Fe_2O_3}$ ceramic system at $x = 0.1$ and ball-milling time of **a** 0 h; **b** 2 h; **c** 4 h; **d** 8 h; **e**12 h

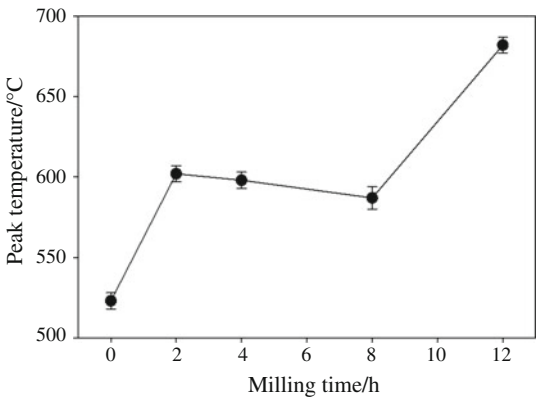

Fig. 4 Peak temperature extracted from DSC curves of $x\mathrm{TiO_2(a)} \cdot (1-x)\alpha\text{-}\mathrm{Fe_2O_3}$ ceramic system at $x = 0.5$ as a function of ball-milling time

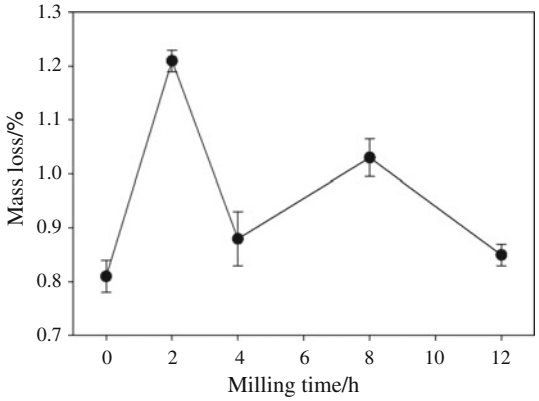

Fig. 5 Mass loss extracted from TG curves of $x\mathrm{TiO_2(a)} \cdot (1-x)\alpha\text{-}\mathrm{Fe_2O_3}$ ceramic system at $x = 0.5$ as a function of ball-milling time

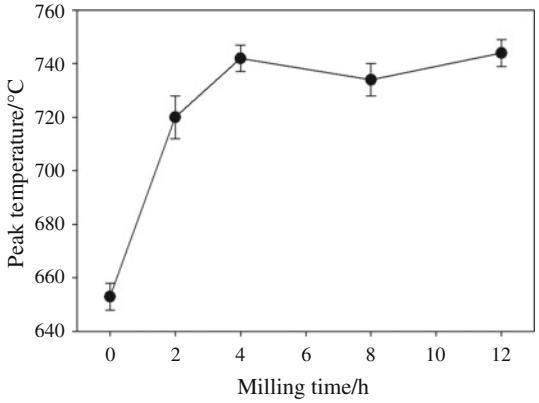

Fig. 6 Peak temperature extracted from DSC curves of $x\mathrm{TiO_2(a)} \cdot (1-x)\alpha\text{-}\mathrm{Fe_2O_3}$ ceramic system at $x = 0.9$ as a function of ball-milling time

each sample is slightly higher than that of 0 h milling sample, indicating the enhancement of hematite decomposition in these samples after milling, compared to the manually ground sample. XRD results showed that anatase gradually evolved into hematite lattice, and Mössbauer [12] results showed there are different types of magnetic species. The thermal behavior of these samples is different from that of original hematite. The dramatic decrease in enthalpy value is possibly due to Ti substitution of Fe in hematite lattice after ball-milling, which suppresses the crystallization of hematite and anatase fine particles. The overall trend of decrease in enthalpy values as function of milling time also confirmed that the increase of Ti substitution of Fe in hematite lattice (as shown by Mössabuer spectra) increases the $\mathrm{Fe_2O_3}$–$\mathrm{TiO_2}$ solid–solid interaction, which in turn suppresses the crystallization of fine particles.

Figure 6 shows peak temperature extracted from the DSC curves of $x\mathrm{TiO_2(a)} \cdot (1-x)\alpha\text{-}\mathrm{Fe_2O_3}$ ($x = 0.9$) samples as a function of ball-milling time for 0, 2, 4, 8, and 12 h, respectively. At 0 h milling time, the DSC curve is similar to that of pure anatase, but with a lower peak temperature at 653 °C and lower intensity of heat flow, indicating the effect of small amount of hematite on the thermal behavior of anatase. The integration of this peak gives an enthalpy value of 1.2 kJ g^{-1}. The smaller enthalpy value and lower peak temperature in the DSC curve may characterize solid–solid interactions between hematite and anatase. Figure 7 shows mass loss extracted from the TG curve of $x\mathrm{TiO_2(a)} \cdot (1-x)\alpha\text{-}\mathrm{Fe_2O_3}$ sample ($x = 0.9$) as a function of milling time. For 0 h ball-milling sample, 0.57% mass loss can be observed with temperature up to 600 °C, which is much smaller than that of the original anatase (10.36%). Compared to original anatase, the decrease in mass loss in the TG process for this sample is possibly due to the water loss during manually mixing and grinding process of hematite and anatase.

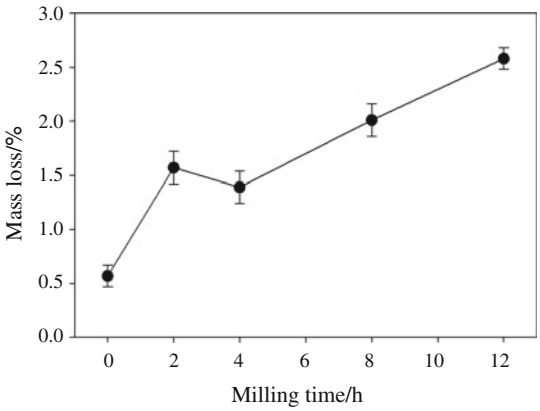

Fig. 7 Mass loss extracted from TG curves of $x\mathrm{TiO_2(a)} \cdot (1-x)\alpha\text{-}\mathrm{Fe_2O_3}$ ceramic system at $x = 0.9$ as a function of ball-milling time

After ball-milling for 2, 4, 8 and 12 h, the DSC curves of $x\mathrm{TiO_2(a)} \cdot (1\text{-}x)\alpha\text{-}\mathrm{Fe_2O_3}$ ceramic system ($x = 0.9$) change dramatically compared to the sample for 0 h milling, indicating the strong effect of ball-milling on the thermal behavior of $x\mathrm{TiO_2(a)} \cdot (1\text{-}x)\alpha\text{-}\mathrm{Fe_2O_3}$ system. The DSC curves show smaller enthalpy values, with values of 118 J g^{-1} and 61 J g^{-1} after 4 h and 8 h milling time, respectively. While the peak temperature extracted from DSC curves showed the increasing trend with the milling time (Fig. 6), from the mass loss as a function of milling time (Fig. 7) it was found that the mass loss increased as a function of milling time. The increase in mass loss is possibly due to the decrease in particle sizes of samples after long milling time, which will absorb more water when exposed to air. The decrease in particle size is in agreement with the XRD results [12] that the diffraction peak is broadened, although most of the anatase phase converted to rutile phase after 12 h milling time.

Conclusions

Anatase-doped hematite $x\text{TiO}_2(\text{a}) \cdot (1-x)\alpha\text{-Fe}_2\text{O}_3$ ($x = 0.1$, 0.5 and 0.9) ceramic system was synthesized by ball-milling methods. The simultaneous DSC–TG investigation has demonstrated that there is a strong effect of ball-milling on the thermal behavior of $x\text{TiO}_2(\text{a}) \cdot (1-x)\alpha\text{-Fe}_2\text{O}_3$ ceramic system. For $x = 0.1$ and 0.5, due to the gradual Ti substitution of Fe in the hematite lattice and smaller particle size after ball-milling, the decomposition of hematite is enhanced, while the crystallization of hematite was suppressed and exhibited a drop in the enthalpy values, due to the anatase-hematite solid–solid interaction. For $x = 0.9$, the thermal behavior of $x\text{TiO}_2(\text{a}) \cdot (1-x)\alpha\text{-Fe}_2\text{O}_3$ showed smaller enthalpy value of anatase crystallization due to the enhancement of hematite–anatase interaction after the milling process; the mass loss upon heating increased as a function of milling time since more water content was absorbed by samples with smaller particle sizes.

Acknowledgements This work was supported by the National Science Foundation under grant number DMR-0854794.

References

1. Krishnamoorthy S, Rivas JA, Amiridis MD. Catalytic oxidation of 1, 2-dichlorobenzene over supported transition metal oxides. J Catal. 2000;193:264–72.
2. Sorescu M, Diamandescu L, Tomescu A, Tarabasanu-Mihaila D, Teodorescu V. Structure and sensing properties of 0.1SnO2–0.9-Fe2O3 system. Mater Chem Phys. 2008;107:127–31.
3. Birkefeld LD, Azad AM, Akbar SA. Carbon monoxide and hydrogen detection by anatase modification of titanium dioxide. J Am Ceram Soc. 1992;75:2961–8.
4. Bahnemann DW, Bockelmann D, Goslich R, Hilgendorf M, Weichgrebe D. Photocatalytic detoxification of polluted aquifers: novel catalysts and solar applications. In: Olliis DF, Al-Ekabi H, editors. Photocatalytic purification and treatment of water and air. Amsterdam: Elsevier; 1993. p. 301–20.
5. Schrauzer GN, Guth TD. Photolysis of water and photoreduction of nitrogen on titanium dioxide. J Am Chem Soc. 1977;99: 7189–93.
6. Litter MI, Navio JA. Comparison of the photocatalytic efficiency of TiO_2, iron oxides and mixed Ti(IV)/Fe(III) oxides: photo-degradation of oligocarboxylic acids. J Photochem Photobiol A: Chem. 1994;84:183–93.
7. Palmisano L, Schiavello M, Sclafani A, Matin C, Matin I, Rives V. Surface properties of iron-titania photocatalysts employed for 4-nitrophenol photodegradation in aqueous TiO_2 dispersion. Catal Lett. 1994;24:303–15.
8. Choi W, Termin A, Hoffmann MR. The role of metal ion dopants in quantum-sized TiO_2: correlation between photoreactivity and charge carrier recombination dynamics. J Phys Chem. 1994;98: 13669–79.
9. Yuan ZH, Zhang LD. Influence of $ZnO + Fe_2O_3$ additives on the anatase-to-rutile transformation of nanometer TiO_2 powders. Naostructured Mater. 1998;10:1127–33.
10. Campostrini R, Ischia M, Palmisano L. Pyrolysis study of sol-gel derived TiO_2 powders: part I. TiO_2-anatase prepared by reacting titanium (IV) isopropoxide with formic acid. J Therm Anal Calorim. 2003;71:997–1021.
11. Lagashetty A, Vijayanand H, Basavaraja S, Bedre MD, Venkataraman A. Preparation, characterization, and thermal studies of γ-Fe_2O_3 and CuO dispersed polycarbonate nanocomposites. J Therm Anal Calorim. 2010;99:577–81.
12. Sorescu M, Diamandescu L, Sanns A, Proch D, Wood J, Teodorescu VS. Synthesis and characterization of ceramic nanoparticles system based on anatase-doped hematite. Res Lett Mater Sci. 2007;48962:1–5.
13. Lin CR, Chiang RK, Cheng CJ, Lai HY, Lyubutin IS, Alkaev EA. Preparation of magnetite nanoparticles by thermal decomposition of hematite powder in the presence of organic solvent. In: Pappas DP, editor. Nanoscale magnetics and device applications. Mater Res Soc Symp Proc. 2007;998E:0998-J08-05.
14. Udalov YP, Mikhailo MN, Smirnov VV, Sharov DY. Interaction of molten iron with materials containing hematite. Glass Phys Chem. 2008;34:305–12.